



BEHAVIOR OF STEEL MOMENT FRAMES WITH DEEP COLUMN SECTIONS UNDER SEISMIC LOADING

T.-Y. Wu⁽¹⁾, S. El-Tawil⁽²⁾, J. McCormick⁽³⁾

⁽¹⁾ PhD Candidate, Dept. of Civil & Environmental Engineering, University of Michigan, Ann Arbor, MI 48109, tungyuwu@umich.edu

⁽²⁾ Professor and Assoc. Dept. Chair, Dept. of Civil & Environmental Engineering, University of Michigan, Ann Arbor, MI 48109, eltawil@umich.edu

⁽³⁾ Assoc. Professor, Dept. of Civil & Environmental Engineering, University of Michigan, Ann Arbor, MI 48109, jpmccorm@umich.edu

Abstract

The behavior of a four-story steel special moment frame (SMF) subjected to various levels of seismic excitation is investigated computationally. The frame employs deep column sections designed in accordance with current design criteria. The structural system is represented by a detailed finite-element model, validated using available experimental data and capable of accounting for the influence of local buckling as well as lateral torsional buckling behavior of the steel columns. The effect of: 1) three different laterally braced conditions for the columns, and 2) three different levels of gravity load on the collapse response are parametrically investigated. It is shown that when the gravity axial load ratios are larger than 20% of the yield capacity, the columns become significantly more susceptible to severe local and global buckling, which can lead to vertical progressive collapse.

Keywords: Steel Moment Frames; Collapse Capacity; Finite Element; Deep Column.



1. Introduction

Seismic provisions that took effect in the late 1990s pushed engineers to start using deep wide flange sections for columns. Deep sections are those with a depth of 24 inches (W24) or greater. The vulnerability of deep columns to torsional demands resulting from the formation of plastic hinges at adjacent moment connections raised the concern of researchers. Efforts documented in [1], [2], and [3] suggested that the concerns were generally unfounded, but the column behavior in these early studies was not fully assessed. For example, the columns in the test conducted were not axially loaded.

Due to scarce information on deep column behavior under the combined effect of axial and lateral loading, NIST proposed a comprehensive computational and experimental research plan to study the seismic performance of individual members, subassemblies, and overall systems that employ deep, slender beam-columns [4]. Since then, several researchers have conducted analytical and experimental studies in this area, e.g. [5], [6], and [7]. While the boundary conditions, loading schemes, and failure criteria utilized in these efforts are different, the new studies concur that many deep sections considered to be highly ductile under current provisions cannot achieve 4% lateral drift ratio under the designated cyclic lateral loading protocol when the axial load ratio P/P_y is larger than 0.2, where P is the axial force on the column and P_y is the axial yield strength of the column cross section, i.e., $P_y = AF_y$. Modifications to current design regulations and design aids were proposed in [5] and [6]. In spite of these recent efforts, the seismic behavior of steel special moment frames (SMF) with deep columns remains unclear. In particular, the connection between individual member and overall system behaviors needs to be established.

Given the above motivation, the objective of this study is to better understand the effect of deep columns on the overall seismic performance of a SMF system. A detailed finite element model of a four-story SMF is developed first and validated using available experimental data. A parametric study is then performed to investigate the influence of different laterally braced column conditions and axial load ratios on collapse behavior.

2. Finite Element Model Development

2.1 Modeling Approach

A four-story building that was designed in [8] using then current design criteria ([9], [10], and [11]) is considered in this study. The designed SMF employs deep column sections. The building has three-bay perimeter steel SMFs on each side and is designed with reduced beam sections (RBS). The plan view of the building and elevation view of the SMFs are shown in Fig. 1. The site class of the building is D and the seismic design category (SDC) is D_{max} . The SMFs are designed to resist all the seismic forces of the building and the gravity loads of the tributary area indicated in Fig. 1. The section of 1st-story columns is W24x103 with a flange width-to-thickness ratio ($b_f/2t_f$) of 4.59, a web width-to-thickness (h/t_w) of 39.2, and a member slenderness ratio (L/r_y) of 80.0, where L is the unbraced length of the columns. This section is defined as a highly ductile member when the axial load ratio (P/P_y) is less than 0.8 according to [9]. The columns are spliced at the third story.

The finite element model of the SMF shown in Fig. 1b is created using the commercial software HyperMesh [12] and analyzed using the commercial code LS-DYNA [13]. The SMF is discretized by using fully integrated shell elements (ELFORM 16 [14]) with the same mesh in [5], as shown in Fig. 2b. The material properties of A992 with the expected material strength ratio of 1.1 are converted to true stress-true strain values using the model proposed in [15]. This true stress-strain data is used to calibrate the strain rate-independent, nonlinear, kinematic hardening material model (LS-DYNA MAT_153 [16]) that is assigned to the shell elements. In order to consider P-Delta effects, a leaning column (Fig. 2a) is used and connected to the SMF by truss members, and a gravity load equal to half of the building minus that distributed to the SMF system is applied at each floor of the leaning column. Rayleigh damping of 2.5% is assumed at the first mode period (1.67 s) of the SMF for the analysis.

2.2 Validation

The finite element model is validated using experimental data in [7], where the collapse response of W24 sections subjected to axial force and lateral deformation was investigated. Finite element models were created using the same modeling technique as the one described in Section 2.1, except that the material properties obtained from the tensile coupon test in [7] are used instead. Only in-plane rotation (R_y) is allowed at the bottom end of the column

while the in-plane displacement (U_x), vertical displacement (U_z), and in-plane rotation (R_y) are allowed at the top end of the column. The in-plane rotation is controlled by two vertical elastic springs added at each end of the column, and the stiffness of the springs was calibrated to match the column's lateral stiffness observed in the test. An initial imperfection with an out-of-plane sinusoidal shape is employed for the column, and the maximum deflection at the mid-height is $L/1000$ which corresponds to the maximum out-of-straightness tolerance permitted [17]. The details of the finite element validation model are shown in Fig. 3.

The loading scheme consists of applying a designated constant axial load to the top end of the column first and then a cyclic lateral drift history based on the required loading sequence for beam-to-column moment connections in [9], which is consistent with the loading protocol used in [7].

Due to limited space, only the comparison of hysteresis responses and failure modes of the W24x131 column with $C_a = 0.2$ (Specimen 2L) is shown in Fig. 4. As can be seen from the figure, the maximum lateral force, the initial and post-yield lateral stiffness, and the strength degradation rates obtained from the computational models are similar to those measured experimentally. In addition, the local buckling shape, length, and occurrence time are well captured by the models and match the description in [7]. The final failure mode of the specimen is also correctly simulated by the finite element model. These reasonable results are typical of the other validation studies.

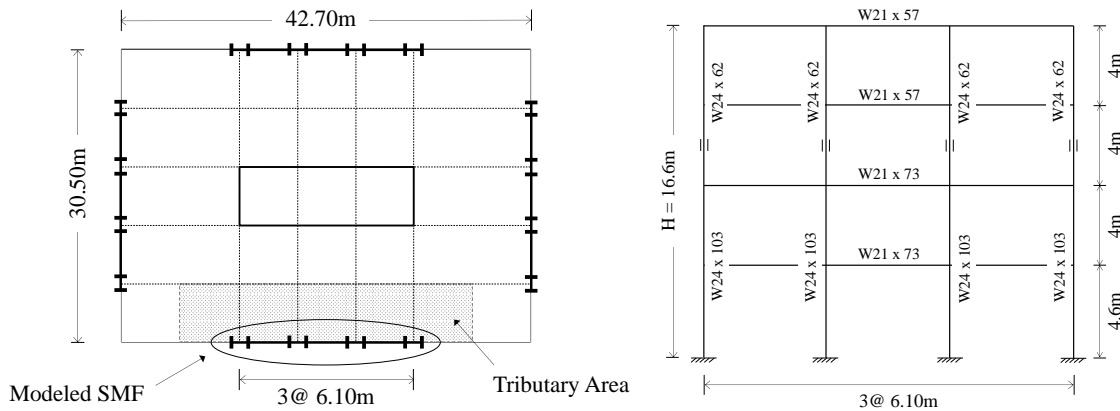


Fig. 1 – (a) Plan view of the four-story building [8]; (b) elevation view of the modeled SMF

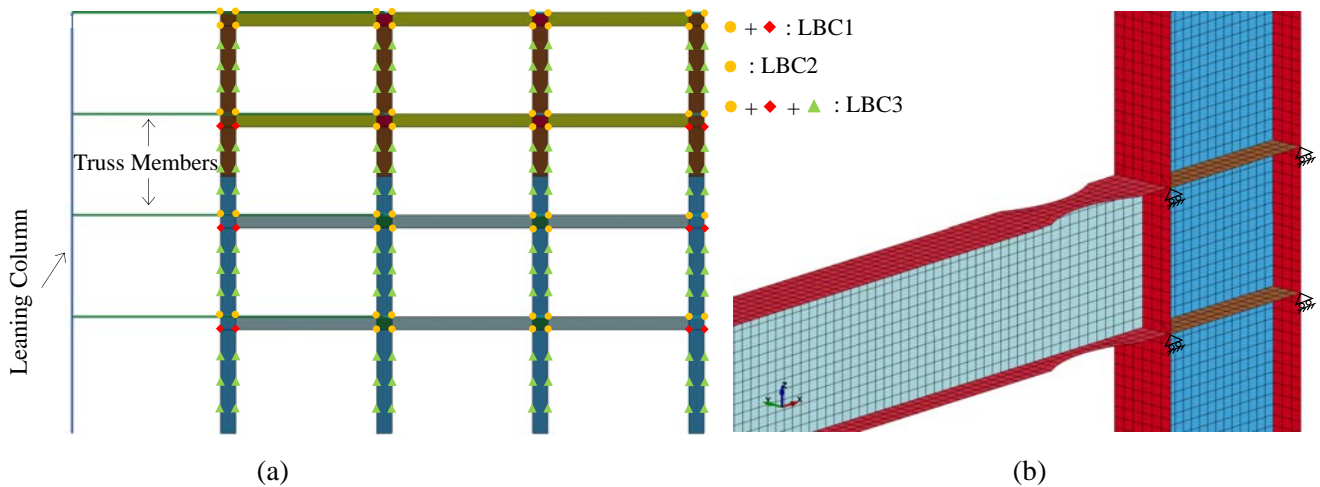


Fig. 2 – Finite element model of SMF (a) details; (b) elevation view

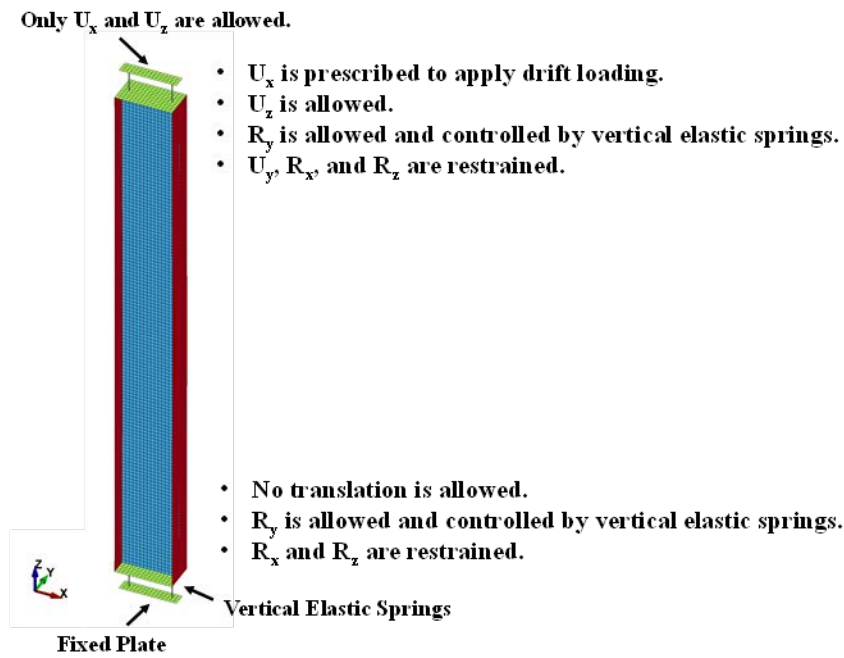


Fig. 3 – The mesh and boundary conditions of the finite element validation model

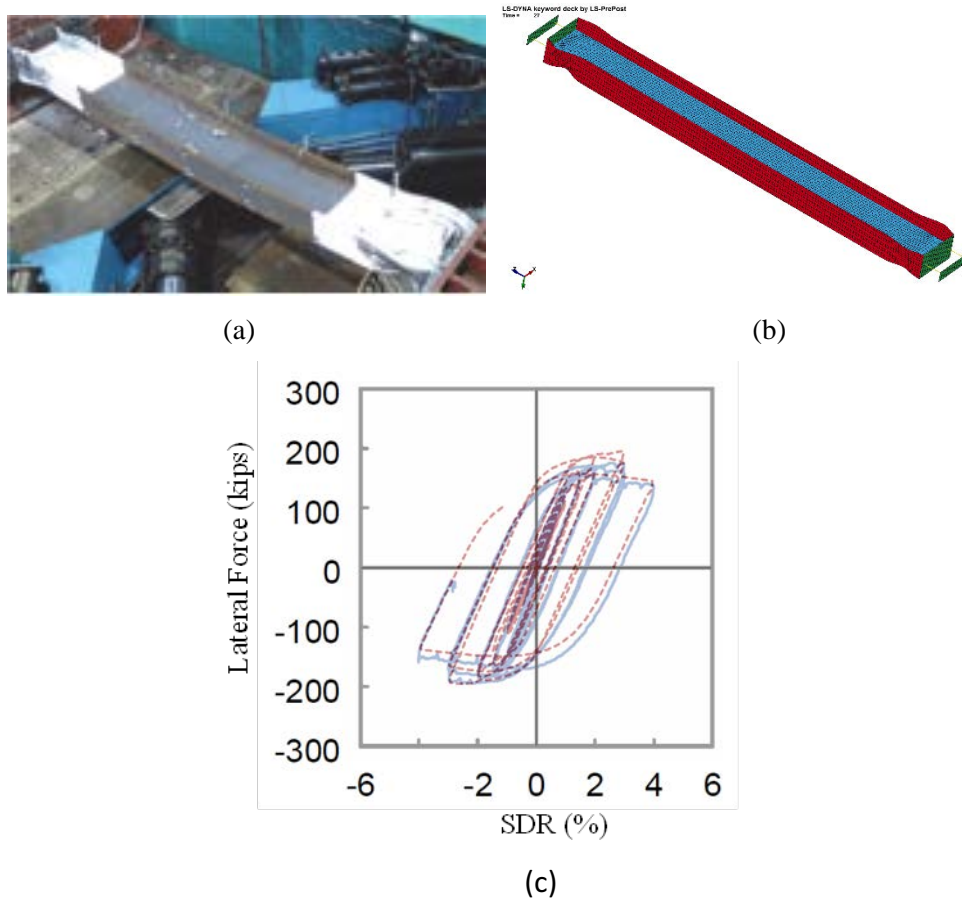


Fig. 4 – (a) Deformed shapes of the columns in the experiment [7] ; (b) deformed shapes of the columns in the finite element models; and (c) hysteresis responses of finite element models (dashed lines) and experimental results (solid lines) [7]



3. Model Setup

3.1 Laterally braced condition and tributary gravity loads

Lateral bracing is achieved by preventing out-of-plane translation at key nodes (Fig. 2b). The top flanges of the steel beams are laterally braced at locations with a spacing L_b that satisfies the requirement for highly ductile members in [9]. For beam-to-column connections, column flanges are laterally braced at the levels of both the top and bottom beam flanges. The model with these bracing conditions is designated LBC1.

To investigate the effect of bracing, two other SMF frame models are created. According to [9], when the column-beam moment ratios of exterior columns are greater than 2.0, column flanges are allowed to be laterally braced only at the level of the top beam flanges. In this calculation, the nominal and expected flexural strengths of the columns and beams, respectively, are used. In beam-to-column connections in the second frame, which satisfies this limit, exterior columns are braced at the level of the top beam flanges only, i.e. no bracing is placed at the bottom flange level. The second frame is designated LBC2. The third frame, named LBC3, is similar to the first, but has additional lateral bracing for all columns at 0.25, 0.5, and 0.75 column height. The locations of lateral bracing of column flanges for above three frames are shown in Fig. 2a.

The other key parameter in this study is the axial load ratio (P/P_y). The axial load ratio induced by the tributary gravity load shown in Fig. 1 is 0.20 for the exterior columns. These values are arbitrarily adjusted to explore the effect of (P/P_y) on the collapse behavior of the SMF. The value is increased to 0.30 to reflect a greater tributary area and reduced to 0.12 to reflect a smaller tributary area. In both cases, the total mass of the SMF remains unchanged, and, in turn, the seismic force applied to the SMF.

3.2 Collapse criteria

Three criteria are used to define the collapse of the SMF under seismic loading: (1) an increase of more than 2% in the maximum story drift ratio within a 10 second period after 95% of the Arias intensity [18] ($t_{IA=95\%}$) has been delivered; (2) the maximum story drift ratio exceeds 10%; and (3) one or more columns lose their axial capacity to carry gravity loads.

The first criterion is intended to signal that a P-Delta collapse will occur without actually modeling the entire event to reduce computational cost. Fig. 5a shows the 1st story drift ratio (1st-SDR) time history within a 10 second period after $t_{IA=95\%}$ for a SMF subjected to the record at Canyon Country station from the 1994 Northridge earthquake scaled to different spectral accelerations corresponding to the first mode period of the SMF with 5% damping, i.e. $S_a(T_1, 5\%)$. Fig. 5b plots the increase in 1st-SDR as noted above versus spectral acceleration and shows that the higher the spectral acceleration, the faster the increase in the rate of the drift ratio. The rapid increase of story drift ratio indicates that the SMF is suffering from severe strength and stiffness deterioration due to seismic loading and is on its way to collapse. Based on experience with numerous simulations all the way up to full collapse, an increase of 2% in drift ratio in the selected 10 second window was found to be a sufficient signal for impending P-Delta collapse.

The 10% maximum drift ratio limit, i.e. the second criterion, is used to detect sidesway collapse when the SMF is subjected to long duration records, which are computationally challenging to address. This drift level has been used by [19] to also signal collapse.

Unlike sidesway collapse, vertical progressive collapse of the SMF is readily identified because of the sudden loss of column axial capacity. At the initiation of progressive collapse, one of the exterior 1st story column first loses its ability to carry gravity load due to global and local instability resulting from cyclic loading and the increased axial loading due to the seismic overturning moments. The redistribution of the gravity load originally supported by the failed column promotes failure in adjacent structural members leading to a progressive collapse scenario. The progression is rapid and can be easily observed in the axial load history of the columns, as shown in Fig. 6. In Fig. 6, columns A1 and D1 experience load reversals due to routine seismic loading. As D1 fails, it sheds its axial load to C1. With the loss of D1, the redistribution of gravity load and reversal of loading induced by overturning moment drastically increase the demands on A1 and C1 and rapidly lead to the failure of the SMF. Therefore, vertical progressive collapse can be identified once redistribution of gravity load and shift of load reversal are observed from the axial load history of the columns.

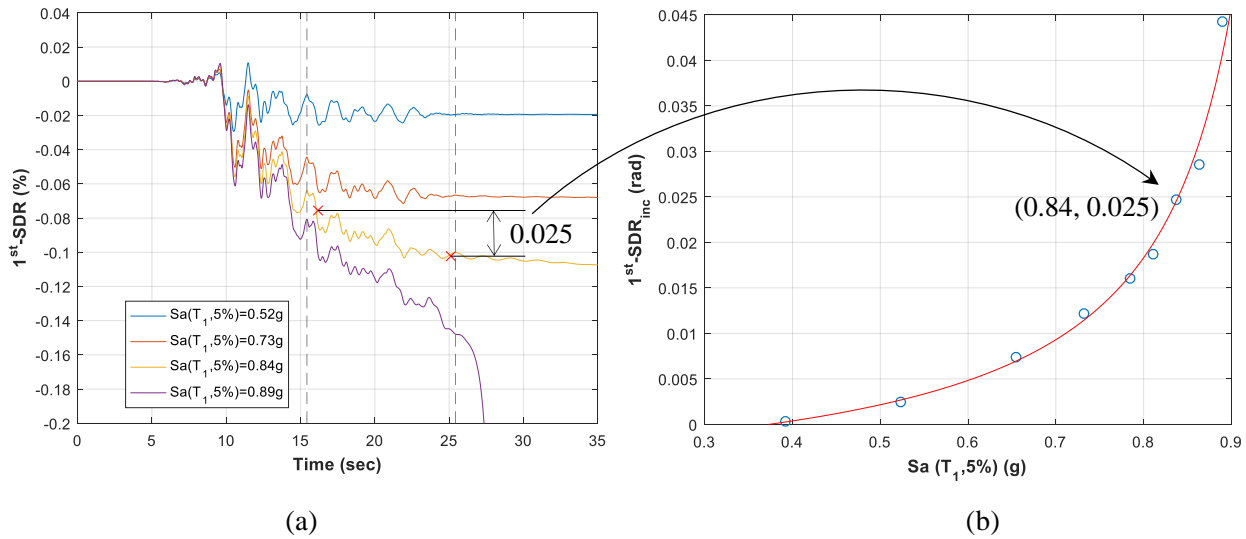


Fig. 5 – (a) Inter-story drift ratio history for 1st floor; (b) increased amount within 10 seconds after 95% of the Arias intensity has been delivered [Canyon Country station from the 1994 Northridge earthquake with different spectral acceleration (LBC1, $P/P_y = 0.12$)]

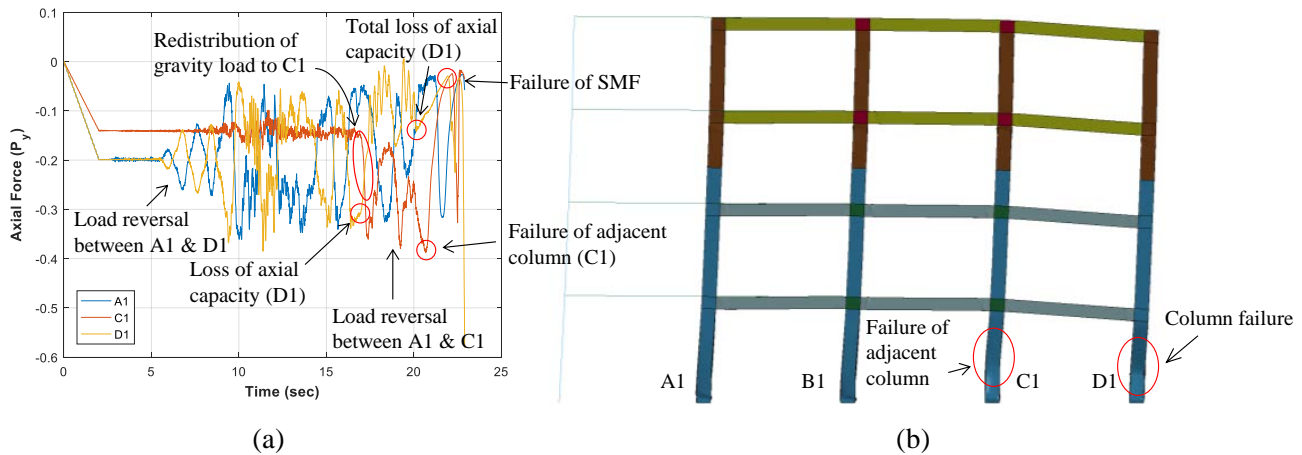


Fig. 6 – (a) Axial load history of 1st-story columns; (b) vertical progressive collapse of the SMF subjected to the record at Bolu station from the 1999 Düzce earthquake with $S_a(T_1, 5\%) = 0.97g$ (LBC1, $P/P_y = 0.20$)

4. Results of Parametric Study

The first component of the first three motions in the Far-Field ground motion record set in [20] are listed in Table 1 and used to study the influence of lateral bracing and column axial load on the collapse behavior of the SMF. The collapse intensity $S_{CT}(T_1, 5\%)$ of the SMF under different conditions for each record is obtained by using incremental dynamic analysis (IDA [19]) when the scaled intensity causes collapse of the SMF according to the criteria defined in Section 2.3. The analysis results are summarized in Table 2 and Fig. 7.

4.1 $P/P_y = 0.20$

Under sufficiently high scaling of the spectral acceleration, the SMF fails due to sidesway collapse for records #1 and #2 regardless of the laterally braced condition. A multi-story mechanism was observed as shown in Fig. 8a, which means that the capacity of the SMF is almost fully developed. The maximum drift ratio that the SMF can reach is 9.0% in these situations. This ratio is much higher than the ones seen in previous studies, e.g. [5], [6], and [7], for individual columns. The difference is that members in [5], [6], and [7] were subjected to symmetric cyclic



loading, whereas in the present study, the first floor columns saw more of a sustained monotonic loading effect during the failure cycle for records #1 and #2. An explanation for this phenomenon can be seen in the 1st-floor drift ratio history shown in Fig. 5. As can be seen from Fig. 5, while the drift history includes many cycles, most cycles do not oscillate about the origin. Instead, the cycles oscillate only on one side due to the P-Delta effect and ratchet up almost monotonically. This situation limits the damage to only one side of the column section, as shown in Fig. 8b, protecting the other side and allowing the SMF to support gravity load at higher drift ratios than under the symmetric cyclic loading protocols used in [5], [6], and [7].

Unlike records #1 and #2, record #3 resulted in vertical progressive collapse as shown in Fig. 6 for the SMFs with LBC1 and LBC2. The drift ratio history of record #3 has more large-cycles that oscillate across the origin, promoting early global failure of the columns. The maximum drift ratio that the SMFs can reach is 4.7% and 4.4% for LBC1 and LBC2, respectively. For the SMF with LBC3 under record #3, sidesway collapse occurs since global failure of columns is effectively prevented by the lateral bracing along the height of the columns.

The collapse intensities of the SMF with LBC1 and LBC2 are essentially similar (within 3%) as shown in Table 2 for records #1 and #2. However, when the SMF is subjected to record #3, it fails due to vertical progressive collapse. In this case, the collapse intensity for LBC1 is 10% higher than for LBC2. The additional bracing at the beam-column connection is able to improve column capacity and helps increase the collapse resistance of the SMF. For LBC3, the collapse intensity is 14% larger than the ones for LBC1. Although this result indicates some benefit for along-height bracing, the benefit appears small for the cost and practical difficulty associated with bracing the columns so extensively.

4.2 $P/P_y = 0.12$

When the axial load ratio decreases from 0.20 to 0.12, all SMF models, i.e. LBC1, LBC2, and LBC3, fail due to sidesway collapse for all records. Compared to the case where $P/P_y = 0.20$, the maximum drift ratio of the SMF increases from 8.3% to 8.8% for record #1 and #2 and from 5.2% to 6.6% for record #3 (averaged over all three LBCs). In addition, the collapse intensity increases 4% for record #1 and #2 and 28% for record #3 (averaged over all three LBCs). The significant increase for record #3 is attributed to a change in failure mode, i.e. from vertical progressive collapse to sidesway collapse. It shows that when the axial load ratio is 0.12, sidesway collapse is the dominant failure mechanism for the SMF used in this study and, therefore, the effect of the additional lateral bracing on the performance of the SMF is minimal in this situation.

4.3 $P/P_y = 0.30$

The collapse capacity of the SMF with LBC1 and LBC2 decreases significantly due to early lateral torsional buckling of the deep columns for all records, leading to vertical progressive collapse of the SMF. The maximum drift ratio that the SMF with LBC1 and LBC2 can attain is 4.3% and 3.0% (averaged over all three records), respectively, and is only 2.8% for the SMF with LBC2 under record #3. This drift capacity is much less than the ones achieved under $P/P_y = 0.20$ prior to collapse. The collapse intensities of the SMF with LBC1 and LBC2 decrease by 27% and 42% (averaged over all three records), respectively, compared to $P/P_y = 0.20$. Moreover, while along-height lateral bracing can prevent columns from global failure, the columns of the SMF with LBC3 under record #3 suffer severe local buckling and eventually lose axial capacity quickly as shown in Fig. 9. The above results show that vertical progressive collapse becomes the dominant failure mechanism when $P/P_y = 0.30$. It appears that $P/P_y = 0.20$ is the transition from sidesway collapse to vertical progressive collapse for the SMF used in this study.

For the SMF with LBC1, the collapse intensity is 29% higher than the ones of the SMF with LBC2 when $P/P_y = 0.30$ (averaged over all three records), indicating that an additional bracing at the level of beam bottom flange has a significant effect on the overall performance of the SMF in this situation. Similarly, the collapse intensity of the SMF with LBC3 increases 36% compared to the SMF with LBC1. This shows that the influence of the laterally braced conditions becomes quite significant when $P/P_y = 0.30$.



Table 1 – Ground motion records used in this study

No.	Event	Station	Component
1	Northridge, 1994	Beverly Hills	9
2	Northridge, 1994	Canyon Country	0
3	Düzce, 1999	Bolu	0

Table 2 – Collapse intensity and attainable maximum SDR of SMFs with different laterally braced conditions and tributary areas under employed ground motion records.

		P_y								
		0.12			0.2			0.3		
		$S_{CT}(T_1, 5\%)$ (g)	SDR_{max} (%)	Failure Mode	$S_{CT}(T_1, 5\%)$ (g)	SDR_{max} (%)	Failure Mode	$S_{CT}(T_1, 5\%)$ (g)	SDR_{max} (%)	Failure Mode
Record #1	LCB1	1.53	8.3	SC	1.48	7.7	SC	1.19	4.8	VPC
	LCB2	1.52	8.3	SC	1.44	7.7	SC	0.87	3.3	VPC
	LCB3	1.68	8.6	SC	1.61	7.5	SC	1.43	6.7	SC
Record #2	LCB1	0.82	9.1	SC	0.77	8.7	SC	0.65	4.9	VPC
	LCB2	0.80	9.3	SC	0.79	8.9	SC	0.52	3.0	VPC
	LCB3	0.80	9.2	SC	0.80	9.0	SC	0.76	8.4	SC
Record #3	LCB1	1.17	6.1	SC	0.94	4.7	VPC	0.51	3.2	VPC
	LCB2	1.24	6.7	SC	0.85	4.4	VPC	0.41	2.8	VPC
	LCB3	1.22	6.9	SC	1.07	6.6	SC	0.87	5.9	VPCLB

*SC: sidesway collapse; VPC: vertical progressive collapse; VPCLB: vertical progressive collapse due to severe local buckling

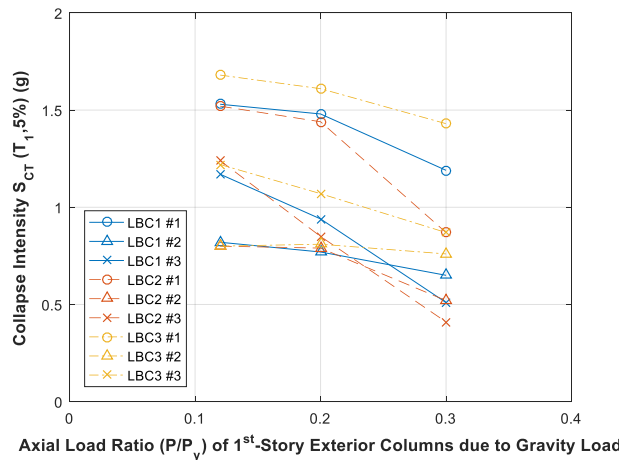


Fig. 7 – Collapse intensity of the SMF subjected to different earthquake records. The blue, orange, and yellow lines represent the SMF with LBC1, LBC2, and LBC3, and the circles, crosses, and triangles represent the SMF under ground motion #1, #2, and #3.

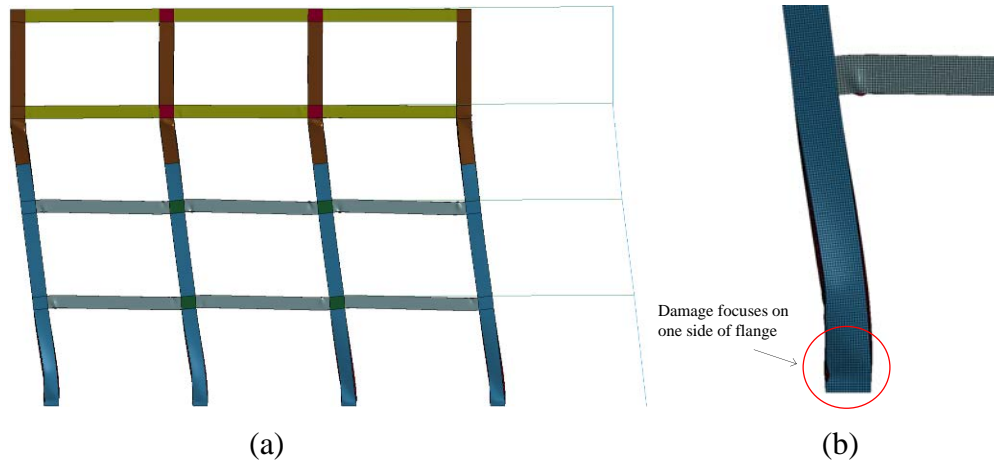


Fig. 8– (a) Multi-story mechanism; (b) flange damage of the SMF subjected to record #1 (LCB1, $P/P_y = 0.20$)

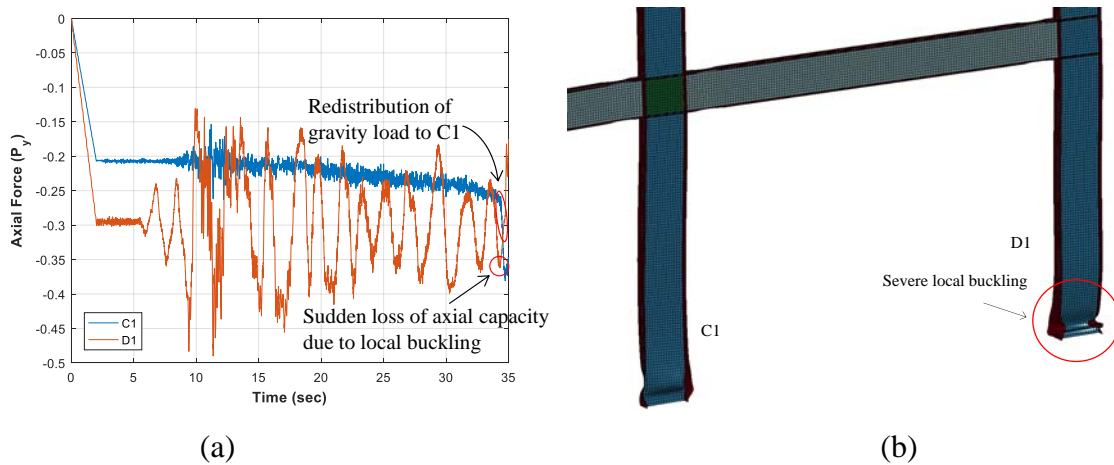


Fig. 9– (a) Axial load history of 1st-story columns; (b) severe local buckling of deep columns when the SMF is subjected to record #3 (LCB3, $P/P_y = 0.30$)

5. Conclusions

The main findings for the specific SMFs and limited number of ground motions employed in this study are summarized as follows.

(1) The collapse mode is quite sensitive to the level of gravity loading on the SMF. Sidesway collapse is the dominant failure mechanism for the SMFs when the axial load ratio is low ($P/P_y = 0.12$). The failure mode starts to transit to vertical progressive collapse as the axial load level increases to $P/P_y = 0.20$ and completely dominates behavior when $P/P_y = 0.30$. Vertical progressive collapse occurs at substantially lower drift ratios than sidesway collapse and is therefore less desirable.

(2) The sustained monotonic loading effect that eventually causes P-Delta collapse appears to protect the column's axial capacity by limiting local buckling damage to only one side of the column. Since previous studies generally employed symmetric loading protocols, which do not accurately model seismic demands at impending collapse, additional research is needed at the component level with demands that more accurately reflect conditions that occur at incipient collapse.

(3) There is no significant difference in performance between the SMFs with different laterally braced conditions when the axial load ratio is 0.12, where sidesway collapse is dominant. The effect of lateral bracing becomes notable when the axial load ratio increases to 0.20. When the axial ratio is 0.30, the removal of the lateral bracing of columns at the level of bottom beam flanges can reduce the collapse intensity of the SMF by 29% and the



addition of the along-height bracing can increase the collapse intensity by 36%. This considerable difference indicates that the laterally braced condition is influential when the SMF is susceptible to vertical progressive collapse.

6. Acknowledgements

This work was supported by the University of Michigan and US NSF grant number CMMI-1344372. Any opinions, findings, conclusions, and recommendations expressed in this paper are those of the authors and do not necessarily reflect the views of the sponsor.

7. References

- [1] Ricles JM, Zhang X, Lu LW, Fisher J (2004): Development of seismic guidelines for deep-column steel moment connections. *ATLSS Report No. 04-13*, ATLSS Engineering Research Center, Lehigh University, Bethlehem, PA, USA.
- [2] Chi B, Uang C. (2002): Cyclic response and design recommendations of reduced beam section moment connections with deep columns. *J. Struct. Eng.*, 10.1061/(ASCE)0733-9445(2002)128:4(464), 464–473.
- [3] Shen JHJ, Astaneh-Asl A, McCallen DB (2002): Use of deep columns in special steel moment frames. *Steel Tip Rep. No. 24*, Structural Steel Educational Council, Moraga, CA, USA.
- [4] NIST (2011): Research plan for the study of seismic behavior and design of deep, slender wide flange structural steel beam-column members. *NIST GCR 11–917-13*, NEHRP consultants Joint Venture.
- [5] Fogarty J, El-Tawil S (2015): Collapse resistance of steel columns under combined axial and lateral loading. *J. Struct. Eng.*, 10.1061/(ASCE)ST.1943-541X.0001350, 04015091.
- [6] Elkady A, Lignos D (2015): Analytical investigation of the cyclic behavior and plastic hinge formation in deep wide-flange steel beam-columns. *Bull Earthquake Eng.*, 13, 1097-1118.
- [7] Uang CM, Ozkula G, Harris J (2015): Observations from cyclic tests on deep, slender wide-flange structural steel beam-column members. *Proc. of Annual Stability Conference*, SSRC, Chicago, IL, USA.
- [8] NIST (2010): Evaluation of the FEMA P695 methodology for quantification of building seismic performance factors. *NIST GCR 10-917-8*, NEHRP consultants Joint Venture.
- [9] AISC (2010): *Seismic Provisions for Structural Steel Buildings. ANSI/AISC 341-10*, American Institute for Steel Construction, Chicago, IL, USA.
- [10] AISC (2010): *Prequalified Connections for Special and Intermediate Steel Moment Frames for Seismic Applications. ANSI/AISC 358-10*, American Institute for Steel Construction, Chicago, IL, USA.
- [11] ASCE (2010): *Minimum Design Loads for Buildings and Other Structures. ASCE/SEI 7-10*, American Society of Civil Engineers, Reston, VA, USA.
- [12] HyperMesh Version 12.0 (2013): Altair Engineering Inc., Troy, MI, USA.
- [13] LS-DYNA (2013): Livermore Software Technology Corp., Livermore, CA, USA.
- [14] Engelmann BE, Whirley RG, Goudreau GL (1989): A simple shell element formulation for large-scale elastoplastic analysis. *Analytical and computational models of shells*, Noor AK, Belytschko T, and Simo JC, ASME, New York, NY, USA.
- [15] Arasaratnam P, Sivakumaran, KS, Tait MJ (2011): True stress-true strain models for structural steel elements. *ISRN Civil Eng.*, 2011, 1–11
- [16] Huang Y., Mahin SA (2010): Simulating the inelastic seismic behavior of steel braced frames including the effects of low-cycle fatigue. *Rep. No. PEER 2010/104*, Pacific Earthquake Engineering Research Center, Univ. of California at Berkeley, CA, USA.
- [17] AISC (2010): *Specification for Structural Steel Buildings. ANSI/AISC 360-10*, American Institute for Steel Construction, Chicago, IL, USA.
- [18] Arias A (1970): A measure of earthquake intensity. In: Hansen RJ, editor. *Seismic Design for Nuclear Power Plants*, pp. 438-483. Cambridge, Massachusetts: MIT Press. 23.



[19] Vamvatsikos D, Cornell CA (2002): Incremental dynamic analysis. *Earthquake Engineering & Structural Dynamics*, 31(3):491–514. DOI: 10.1002/eqe.141

[20] FEMA (2009): Quantification of building seismic performance factors. *Report FEMA-P695*, Federal Emergency Management Agency, Washington, DC, USA.